

Vacuum Ultraviolet Photolysis of Condensed Methyl Chloride in Interstellar Model Conditions and Trapping of Intermediates at Intergrain Interfaces

Bijesh K. Malla, Gaurav Vishwakarma, Soham Chowdhury, and Thalappil Pradeep*



Cite This: *J. Phys. Chem. C* 2023, 127, 24149–24157



Read Online

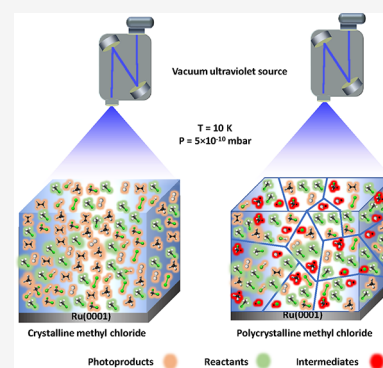
ACCESS |

Metrics & More

Article Recommendations

Supporting Information

ABSTRACT: Photochemistry can generate chemical complexity in an interstellar space. This may occur due to photolysis and associated events that can happen in condensed molecular solids under the prevailing temperature and pressure conditions. In the present study, using reflection absorption infrared spectroscopy (RAIRS), three different condensed phases of methyl chloride ice, namely, amorphous, crystalline, and polycrystalline, were detected in ultrahigh vacuum (UHV) ($p = 5 \times 10^{-10}$ mbar) and cryogenic conditions ($T = 10$ – 90 K). Upon vacuum ultraviolet (VUV) photoirradiation, crystalline methyl chloride formed more photoproducts than amorphous and polycrystalline forms. This unusual finding is attributed to the rapid diffusion and reaction of photochemical intermediates in a crystalline matrix, whereas the intermediates are trapped at grain boundaries in the polycrystalline solid. Normally, the intermediate diffusion is high in the case of the amorphous phase as compared with the crystalline phase. During long-term irradiation, discontinuity in the polycrystalline phase is removed, resulting in enhancement in the formation of photoproducts in the matrix, which was observed by the intensified desorption of photoproducts in temperature-programmed desorption mass spectrometry (TPD-MS). Further, all major and minor neutral photoproducts were detected by highly surface-sensitive Cs^+ ion-based secondary ion mass spectrometry (SIMS).



INTRODUCTION

The fate of molecules in the interstellar medium is largely governed by photochemistry and radiation chemistry.^{1,2} The diversity of such chemistry has contributed to the richness of the interstellar medium (ISM), which is now known to be composed of over 270 species, including simple and complex organic molecules (such as ethylene glycol, benzene, indene, and fullerenes).^{3–6} Such complex molecules are proposed to be formed through radical chemistry in icy grain mantles.⁷ Two of the recent additions to the chemical soup of ISM are methyl chloride (CH_3Cl) and methyl fluoride (CH_3F), which appear to have been formed through photochemistry.⁸ Intriguingly, methyl chloride and other chlorine-bearing organic molecules have also been identified on Mars via the Curiosity rover.⁹ On Earth, the genesis of organohalogen involves geological and biological mechanisms, rendering them potential biomarkers for exoplanets.¹⁰ Despite the evident importance of organohalogen on terrestrial and in extraterrestrial environments, there are no experimental spectroscopic data available on pure and photoirradiated condensed methyl chloride in view of the temperature and pressure conditions prevailing on ISM. Photochemistry of the system will be relevant in affecting the chemical diversity of ISM.

While it is well-known that the amorphous phase of molecules in ISM may undergo a structural change upon annealing to higher temperatures to form their stable

crystalline structures, it is unknown if the crystalline phase is of long-range order or polycrystalline in nature. To the best of our knowledge, there is no report on the phases (crystalline and polycrystalline) of methyl chloride ice based on its IR spectra and no report exists on the analysis of the photoproducts formed by these different ices in ISM conditions. We note that in this literature, ice is a term used for all condensed molecular solids.

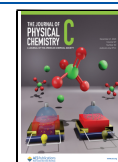
In this study, we present a combined infrared and mass spectrometric investigation of the vacuum ultraviolet (VUV) photochemical transformation of condensed methyl chloride ices in its amorphous, crystalline, and polycrystalline phases. A 1958 study reported the vibrational spectrum of methyl chloride crystallites along with other methyl halides,¹⁴ and several studies reported the IR spectra of amorphous and crystalline methyl chloride.^{11–13} However, the nature of crystallinity, long-range or short-range, is unclear. Here, we characterized the three distinct phases of methyl chloride ice created by three different paths by RAIR spectroscopy and

Received: August 31, 2023

Revised: November 14, 2023

Accepted: November 14, 2023

Published: December 8, 2023



performed a detailed study of the photochemistry of these solids. Upon VUV irradiation with deuterium continuum of 115–400 nm wavelength (Lyman- α), with a peak flux of 6×10^{12} photons $\text{cm}^{-2} \text{s}^{-1}$, condensed methyl chloride ice produces methane (CH_4), ethane (C_2H_6), hydrogen chloride (HCl), dichloromethane (CH_2Cl_2), ethylene (C_2H_4), acetylene (C_2H_2), and ethyl chloride ($\text{CH}_3\text{CH}_2\text{Cl}$). Surprisingly, we found that this photochemical transformation is more facile in the crystalline phase than in the expected amorphous phase. Notably, the concentration of photoproducts is in the order crystalline \geq amorphous $>$ polycrystalline phases. We interpreted the results in view of the rapid diffusion of the intermediates (radicals) of photolysis through the crystalline matrix and the localization of these intermediates at the crystallite grain interfaces in the case of the polycrystalline phase. The consequence of the product accumulation in the crystalline lattice was studied by TPD-MS.

EXPERIMENTAL SECTION

Experimental Setup. In this study, all experiments were carried out in an ultrahigh vacuum (UHV) instrument (with a base pressure of $\sim 5 \times 10^{-10}$ mbar) discussed in detail in our previous literature.^{14,15} The instrument consists of three UHV chambers (namely, ionization, octupole, and scattering) and is equipped with reflection absorption infrared spectroscopy (RAIRS), low energy ion scattering (LEIS), temperature-programmed desorption (TPD) mass spectrometry, and Cs^+ ion-based secondary ion mass spectrometry (SIMS), along with a vacuum ultraviolet (VUV) lamp (Figure 1). Six turbomolecular pumps maintain the vacuum chambers' base pressure, which are supplemented by several oil-free diaphragm

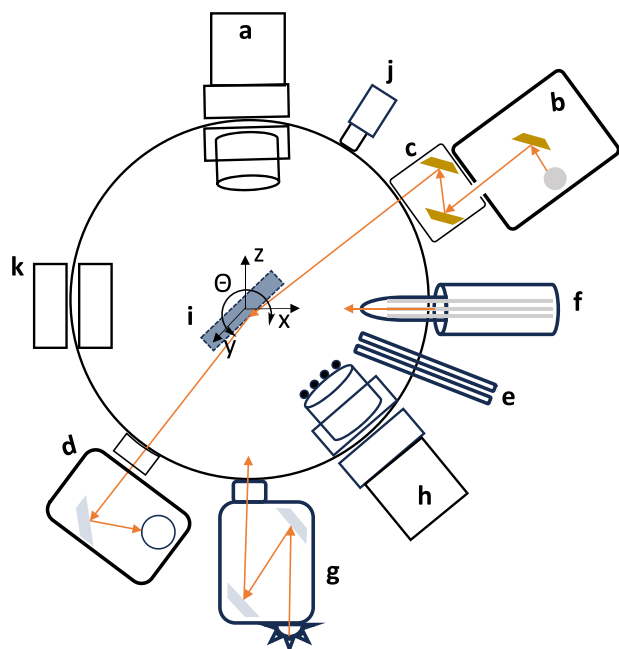


Figure 1. Simplified schematic diagram of experimental setup. (a) Quadrupole mass analyzer. (b) Fourier transmission infrared (FTIR) source. (c) Mirror box. (d) Mercury cadmium telluride (MCT) liquid nitrogen cooled detector. (e) Two sample inlet lines. (f) Low energy alkali ion gun (Cs^+). (g) Deuterium lamp. (h) TPD probe fitted with ionizer and quadrupole mass analyzer and detector. (i) Ru(0001) substrate. (j) Bayard–Alpert (BA) gauge. (k) Low energy ion scattering MS (not used in this study).

pumps. The chamber pressure is monitored by a Bayard–Alpert gauge, controlled by a MaxiGauge vacuum gauge controller (Pfeiffer, Model TPG 256 A).

A highly polished Ru(0001) single crystal was used as the substrate to create thin ice films that was mounted on a copper holder. It was connected to a helium cryostat (Cold Edge technology), which could maintain a temperature as low as 8 K. A resistive heater (25 Ω), controlled by a temperature controller (Lakeshore 336), was used to heat the substrate to 1000 K. The substrate temperature was measured with a K-type thermocouple sensor that has ± 0.5 K accuracy. Repeated heating to 400 K before each vapor deposition ensured a clean surface suitable for the current study. It is worth noting that the surface has a negligible role in the current study, as our experiments were on multilayer ice films (63 monolayer (ML)).

RAIRS and TPD-MS Setup. In this study, the thermal processing of vapor-deposited ice samples was monitored using RAIRS (reflection–absorption infrared spectroscopy) and TPD-MS (temperature-programmed desorption-mass spectrometry). The RAIRS data was collected in the 4000–550 cm^{-1} range with a spectral resolution of 2 cm^{-1} , using a Bruker FT-IR spectrometer called Vertex 70. The ice sample was exposed to an incident angle of $80^\circ \pm 7^\circ$ by focusing the IR beam through a ZnSe viewport. The reflected IR beam from the sample was detected by using a liquid N_2 -cooled mercury cadmium telluride (MCT) detector. To prevent absorption by atmospheric moisture, the IR beam outside the vacuum chamber was purged with dry N_2 . Each RAIR spectrum was obtained by averaging over 512 scans to improve the signal-to-noise ratio. An Extrel quadrupole mass spectrometer was used for TPD-MS in an out-of-sight configuration.

SIMS Setup. The Cs^+ ion-based secondary ion mass spectrometry (SIMS) technique can molecularly identify and monitor the reactions occurring on the surfaces. Cs^+ ($m/z = 133$) was chosen for the ion scattering due to its high depth resolution of 1 bilayer and the ability to monitor neutral chemicals on the CH_3Cl ice surface. We conducted reactive ion scattering experiments with Cs^+ of 60 eV kinetic energy generated by a low-energy alkali gun. The Cs^+ ion collides on the ice surface, adducts with neutral molecules on the surface, and drags them from the surface along its outgoing trajectory, which is known as the RIS (reactive ion scattering) process. The Cs^+ ion adducts with the neutral molecules are driven by an ion-neutral dipole interaction. The mass of the Cs^+ ion adduct was determined with a quadrupole mass analyzer. The mass of the neutral product formed on methyl chloride ice due to photolysis can be identified by subtracting the mass of Cs^+ ($m/z = 133$) from that of the Cs^+ ion adduct.

VUV Source. A deuterium lamp (McPherson, Model 634, with MgF_2 window, 30 W) of vacuum ultraviolet (VUV) range 115–400 nm with a spectral bandwidth of 0.8 nm (shown in Figure S1) was used as the UV light source. The VUV lamp was differentially pumped and attached to the UHV chamber through the MgF_2 window (with a cutoff at ~ 114 nm (10.87 eV)). This design allows the source to effectively emit light at incredibly short wavelengths, reaching as far down as 115 nm. The UV lamp flux was determined by applying the widely used ozone method ($\text{O}_2 \rightarrow \text{O}_3$ conversion), where solid O_2 was VUV photolyzed at 10 K. The average photon flux reaching the ice sample was estimated to be $\sim 6 \times 10^{12}$ photons $\text{cm}^{-2} \text{s}^{-1}$.

Materials and Sample preparation. As received, methyl chloride (Akkaran gas and energy, 99.9% purity) and argon

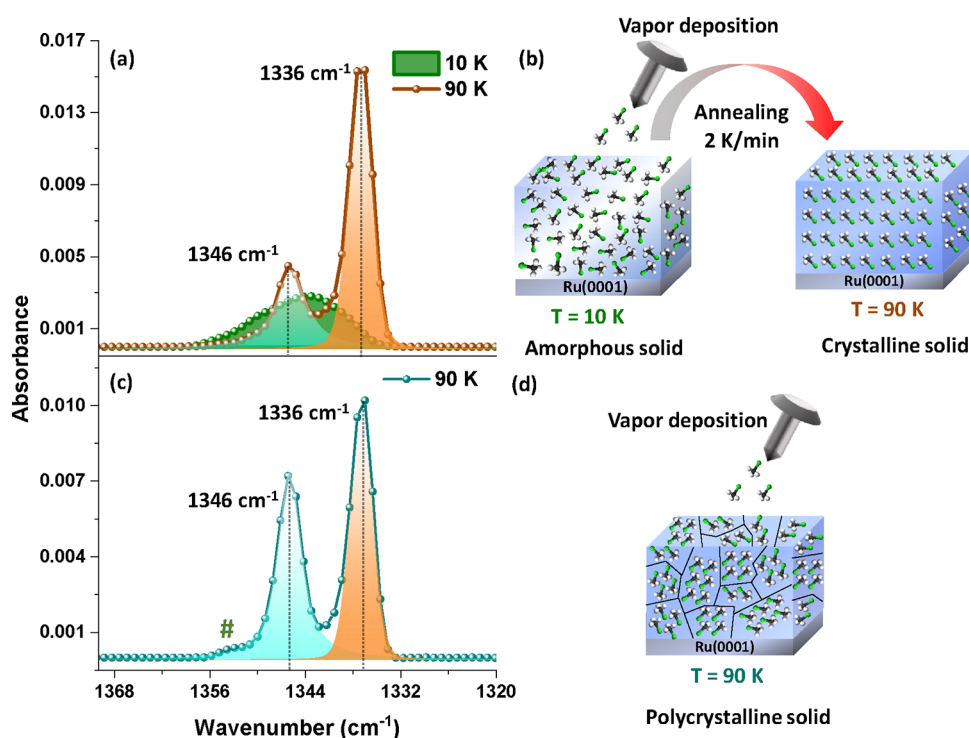


Figure 2. RAIR spectra of amorphous, crystalline, and polycrystalline methyl chloride ice. (a) RAIR spectra of 63 ML of methyl chloride ice at 10 and 90 K in the C–H symmetric mode. For this, methyl chloride vapor was deposited at 10 K on a Ru(0001) substrate and annealed to 90 K with a ramping rate of 2 K/min. (b) Schematic illustration of the phase transition of amorphous to crystalline methyl chloride ice upon annealing. (c) RAIR spectra of 63 ML of methyl chloride ice at 90 K in the C–H symmetric bending mode. For this, methyl chloride vapor was directly deposited at 90 K on the Ru(0001) substrate. (d) Schematic illustration of the formation of polycrystalline methyl chloride ice at 90 K.

(Ar) (Rana industrial gases and products, 99.9% purity) gases were connected to the main chamber through sample inlet lines controlled by high-precision metal leak valves. Millipore water (H_2O of 18.2 M Ω resistivity) was taken in a vacuum-sealed test tube (with a glass-to-metal seal) and was further purified by several freeze–pump–thaw cycles. A source of water vapor was connected to the main chamber through the sample inlet line. It is worth noting that we have two sample inlet lines that were connected to specific gas/liquid in accordance with the distinct experimental requirements.

Methyl chloride ice of 63 ML was prepared by vapor deposition on Ru(0001) at 10 K. The vapor deposition coverage in the case of N_2 (ion gauge sensitivity factor -1) was expressed in ML, assuming 1.33×10^{-6} mbar s = 1 ML, which was estimated to contain $\sim 1.1 \times 10^{15}$ molecules cm^{-2} , as adopted in other reports.^{16–18} Methyl chloride has an ion gauge sensitivity factor of 2.4. To deposit 63 ML of methyl chloride ice, we backfilled the chamber at a pressure of 5×10^{-7} mbar pressure for 5 min. For higher temperature deposition, the Ru(0001) substrate was heated to 90 K with a heating rate of 2 K/min, and methyl chloride was deposited at 90 K. The vacuum gauge was calibrated with nitrogen, and the methyl chloride coverage may be slightly different in view of this uncorrected pressure reading.

For 160 ML of a 2:1 mixture of methyl chloride and water, the chamber was backfilled to a pressure of 4×10^{-7} mbar for methyl chloride and 1×10^{-7} mbar for water for 10 min. For a separate deposition step involving 100 ML of argon (Ar), the chamber was backfilled to a pressure of 5×10^{-7} mbar. This backfilling process was carried out for 4 min and 20 s. Throughout each molecular deposition process, special attention was paid to the ion gauge sensitivity factor to ensure

accurate measurements and control over the deposition. Mass spectra were taken simultaneously during vapor deposition to check the purity and ratio of the deposited molecules. The as-prepared sample was irradiated by a deuterium lamp (McPherson, Model 634, with MgF_2 window, 30 W) in the VUV range of 115–400 nm.

RESULTS AND DISCUSSION

RAIRS Study of Amorphous, Crystalline, and Polycrystalline Methyl Chloride Ice. In this study, we created condensed methyl chloride ice in UHV under cryogenic conditions, as in the interstellar medium, via three different paths, as mentioned above. Figure 2a,c shows the RAIR spectra of 63 ML of methyl chloride ice in the C–H symmetric bending region. In Figure 2a, the broad green spectrum represents the amorphous methyl chloride obtained by vapor deposition at 10 K. Slow annealing of this ice from 10 to 90 K at a rate of 2 K/min causes the rise of two sharp peaks 1346 and 1336 cm^{-1} (cyan and brown color filled, respectively in Figure 2a). This band splitting occurs due to intermolecular coupling within the newly formed crystalline lattice. However, the peak intensity is different.^{19,20} These two split peaks are also observed when methyl chloride is directly deposited at 90 K, as shown in Figure 2c. Further, a tiny peak (marked #) near 1355 cm^{-1} represents methyl chloride gas trapped in the matrix.¹⁹ It is not surprising that a small amount of methyl chloride gas can be trapped in the crystal grains during the direct deposition at 90 K.

However, the peak intensity ratio differs in Figure 2a,c, which may be attributed to the degree of irregularities or random orientations in the crystal lattice. This raises the question if the two nonamorphous solids are identical in their

crystallinity. To resolve this, control experiments were carried out to determine how the intensity of the higher wavenumber peak (or peak ratio) changes with the crystallinity of methyl chloride ice. This is shown by two separate control experiments. One is the annealing rate, a crucial factor in UHV chemistry,^{21,22} and another is the addition of impurities, such as water, in this case. In the first experiment, we deposited 63 ML of methyl chloride ice at 10 K and annealed it to 90 K with a higher annealing rate of 10 K/min. We observed the RAIR spectra of the resulting solid (shown in Figure S2) resemble the spectra observed in the case of direct deposition at 90 K (Figure 2c), including the presence of the gas phase peak (marked by #); however, interestingly, it is absent when slow-annealed (Figure 2a). An increased annealing rate increases the mobility of molecules, so the amorphous solid did not get enough time to form the extended crystal lattice. Next, we deposited 160 ML of 2:1 methyl chloride and water on Ru(0001) and annealed the sample to 90 K with a slow annealing rate of 2 K/min; the obtained IR spectrum (Figure S3) of solid methyl chloride resembles the IR spectra obtained from the randomly oriented crystalline solid (Figure 2c). Here, it is evident that the water impurity within the methyl chloride ice matrix disturbs the extended range of crystallinity. A similar effect is already shown in the dichloromethane case.²⁰ Here, it is concluded that a more ordered crystalline solid can be formed only by slow annealing of the pure ice sample. It is established that the polycrystalline nature of a substance increases upon (a) increasing the annealing rate and (b) introducing an impurity in the sample. We propose that the peak intensities in the C–H symmetric bending mode can be correlated with the extent of the crystalline nature of the methyl chloride solid. Control experiments supported this suggestion. Based on this, we noted that with increased polycrystallinity (irregularities in crystalline), the intensity of the 1346 cm⁻¹ peak increases.

Dows has reported the IR spectra for solid methyl chloride and found that the crystallites are randomly oriented, with the intensity ratio of 1.46¹⁹ for the peaks of 1336 and 1346 cm⁻¹. In our study, we found a ratio of 1.42 for the directly deposited thin film, which supports the polycrystalline nature of methyl chloride. Notably, this ratio is comparable to the ratios of 1.73 and 1.22 in the case of the ice formed via quick annealing and with an impurity, as shown in Figures S4 and S5, respectively. However, the ice formed by slow annealing (Figure 2c exhibits a higher ratio (~3.4), suggestive of a highly crystalline nature (less polycrystalline). A comparison of RAIR spectra of four condensed methyl chloride samples created by four different methods in the C–H symmetric bending region is shown in Figure S4. The annealed sample may be described as a low-polycrystalline or long-range crystalline ice, as depicted in Figure 2b. Thus, the relatively higher intensity of the 1346 cm⁻¹ peak represents the randomness in the crystal lattice. Although our study is not supported by diffraction data, to the best of our knowledge, this is the first report of this nature. We suggest crystalline (less polycrystalline) methyl chloride formation is possible upon slow annealing in a homogeneous environment.

Additionally, the evolution of the C–H stretching and C–H antisymmetric bending modes with increasing temperature for the crystalline solid is shown in Figure S5a,b. In the C–H stretching region, we observed that the broad amorphous peak splits into two peaks at 2961 and 2952 cm⁻¹, while in the C–H antisymmetric bending region, the broad (due to the

amorphous phase) peak splits into 1443 and 1437 cm⁻¹. For the polycrystalline ice, three peaks were observed at 2961, 2955, and 2952 cm⁻¹ in the C–H stretching and 1445, 1441, and 1437 cm⁻¹ in the C–H antisymmetric bending regions (Figure S6). In this experiment, an additional peak appeared in the C–H stretching (2955 cm⁻¹), and the C–H bending regions (1441, 1445 cm⁻¹ peaks were observed in place of 1443 cm⁻¹), which may indicate high irregularities (Figure S6). This may be attributed to molecular interactions between two crystallites in the methyl chloride solid. All the IR peaks for amorphous, crystalline, and polycrystalline methyl chloride ice and gas phases are assigned in Table S1.^{19,23–26}

Photochemistry of Amorphous Methyl Chloride. Such diverse crystallinity can significantly affect the photochemistry in ISM. Photochemical pathways are a succession of photodissociation, radical–radical interactions, and subsequent rearrangements that culminate in the formation of complex organic compounds in ISM.⁷ Therefore, we undertook an investigation of the kinetics of photoproducts formed in these phases of ice. At the outset, we subjected the amorphous methyl chloride ice to VUV light irradiation at 10 K and subsequently analyzed the products using RAIR, SIMS, and TPD-MS.

Figure 3 shows the RAIR spectra of 63 ML of amorphous methyl chloride before and after 60 min of VUV irradiation in

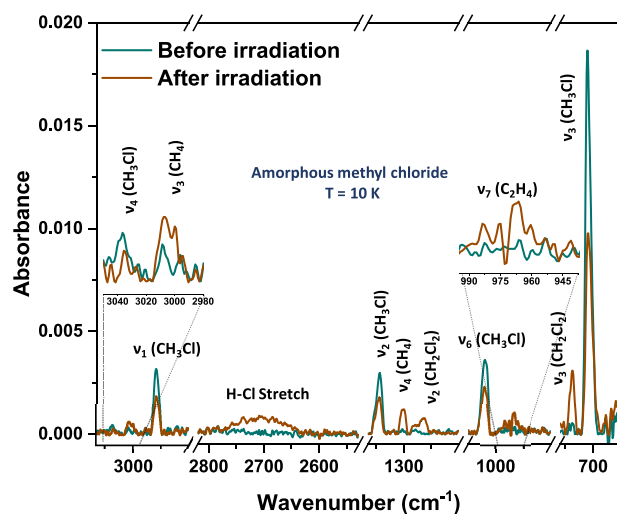


Figure 3. RAIR spectra of 63 ML of methyl chloride before and after irradiation with VUV light at 10 K in the mid-infrared region. Zoomed views of weaker peaks are shown as insets. Methyl chloride vapor was deposited at 10 K on a Ru(0001) substrate and the amorphous methyl chloride ice was photoirradiated for 60 min.

the mid-infrared region. In the IR spectrum shown, methyl chloride is identified by the C–H antisymmetric stretching (ν_4 , 3036 cm⁻¹), C–H symmetric stretching (ν_1 , 2958 cm⁻¹), C–H symmetric bending (ν_2 , 1343 cm⁻¹), C–Cl rocking (ν_6 , 1018 cm⁻¹), and C–Cl stretching (ν_3 , 710 cm⁻¹) modes.^{13,27} New IR peaks arise after 60 min of VUV irradiation due to the formation of new species in the ice matrix. Four major photoproducts were identified by their prominent IR peaks. Methane was identified by C–H antisymmetric stretch (ν_3 , 3009 cm⁻¹) and C–H symmetric stretch (ν_4 , 1302 cm⁻¹); dichloromethane was identified by the C–H symmetric bending (ν_2 , 1263 cm⁻¹), and C–Cl symmetric stretch (ν_3 , 737 cm⁻¹); hydrogen chloride was identified by the H–Cl

stretch ($2780\text{--}2620\text{ cm}^{-1}$) and ethylene was identified by C–H symmetric bending (ν_7 , 965 cm^{-1}).^{27,28} Other than these four, hydrogen and chlorine are two major products that are likely but cannot be detected by our IR spectroscopy. Figure 4

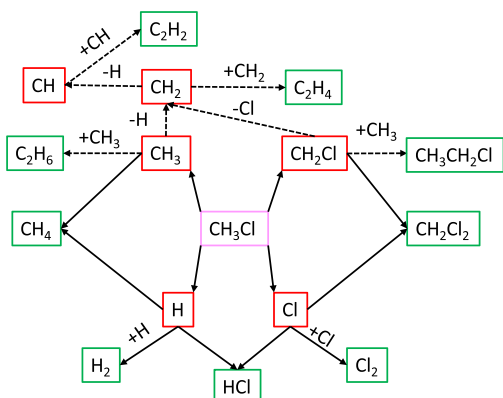


Figure 4. Proposed reaction scheme for the photochemistry of methyl chloride (magenta colored box) displaying major and minor dissociation and radical combination reactions. Green and red color boxes indicate the photoproducts and the intermediates. Solid and dashed arrows denote primary and secondary photodissociation and association processes, respectively.

shows the reaction scheme for all major and minor photoproducts. The proposed reaction scheme elucidates the formation pathways of the observed species resulting from the photoproducted radicals. Here, it is worth noting that all the reaction channels are reversible to a very small extent in the solid ice matrix under continuous VUV irradiation.²⁹ These pathways have been derived from the current knowledge in the literature.^{30–34}

In addition to the photodissociation mechanism, electrons generated from the ruthenium surface (work function-4.7 eV) by photon bombardment may participate in the reaction mechanism. The ejected electron can readily combine with Cl radical to form Cl anion,^{35,36} but this effect of ions will be very minimal. While the photoelectron does indeed play a role,

these electrons have an attenuation length of 2 to 4 ML in side methyl chloride ice.³⁷ To validate this assumption, we conducted a control experiment involving the introduction of 100 ML of argon (Ar) between the Ru(0001) substrate and CH_3Cl ice. Following 60 min of irradiation, we observed the same absolute photoproduct yield within the ice matrix, as illustrated in Figure S7. This implies the photo electron effects are anticipated to be confined to a limited penetration depth within condensed ice.

The minor photoproducts present in very small quantities in the ice matrix cannot be detected by RAIRS and TPD-MS. In this case, SIMS has emerged as one of the most surface-sensitive methods for analyzing molecular solids in UHV^{38,39}; its sensitivity toward surface molecules allows the detection of trace amounts of minor products formed by the photolysis of methyl chloride.⁴⁰ Here, reactive ion scattering (RIS) of Cs^+ makes ionic clusters of the molecular constituents of surfaces. The large peak at $m/z = 133$ is due to Cs^+ (Figure S8), and all other peaks are RIS products of Cs^+ derived from neutral molecules present on the ice surface. Figure 5 shows the Cs^+ scattering spectrum after irradiating amorphous methyl chloride for 60 min. The mass peaks at m/z 183 and 233 are attributed to one and two methyl chloride species picked up by the Cs^+ ion. All of the mass peaks for major and minor products are assigned in the table in Figure 5. The products, methane ($m/z = 149$), acetylene ($m/z = 159$), ethylene ($m/z = 161$), ethane ($m/z = 163$), hydrogen chloride ($m/z = 169$), ethyl chloride ($m/z = 197$), and dichloromethane ($m/z = 217$) were identified. The peaks marked by # is for the isotopic signature of chlorine in the molecules. Peaks at m/z 151 and 201 represent water and water-methyl chloride complexes. A minimal amount of water comes from background deposition, which cannot be avoided in a UHV system. It is important to recognize that the Cs^+ ion is capable of picking up only molecules within the topmost 1 bilayer of the sample. Consequently, the intensity readings for both water and methyl chloride appear identical due to this limitation. The tiny mass peak at $m/z = 165$ shows formaldehyde, which may be due to the reaction between water and methyl chloride on the topmost layer. Additionally, our experimental design

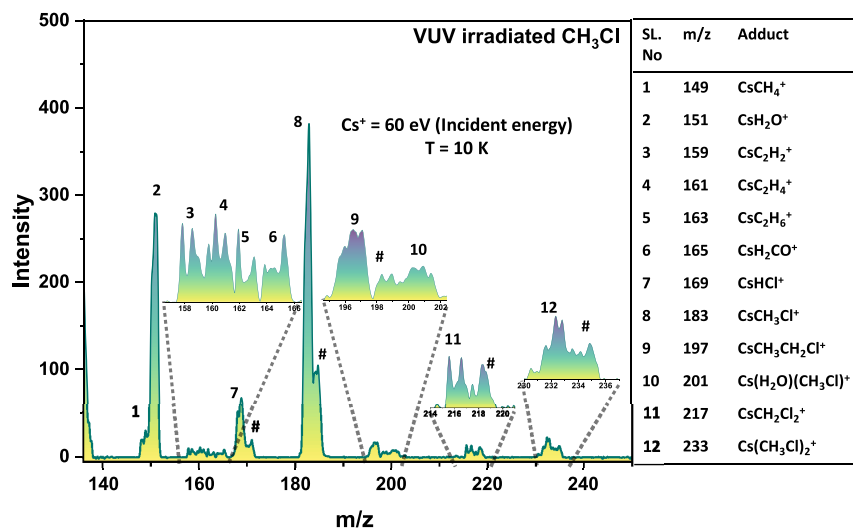


Figure 5. Reactive ion scattering (RIS) mass spectra obtained after 60 min of VUV irradiation of amorphous methyl chloride ice. The mass spectrum of the irradiated ice was obtained by colliding the sample with 60 eV Cs^+ ions at 10 K. All the RIS photoproducts have been assigned, as listed in the table on the right.

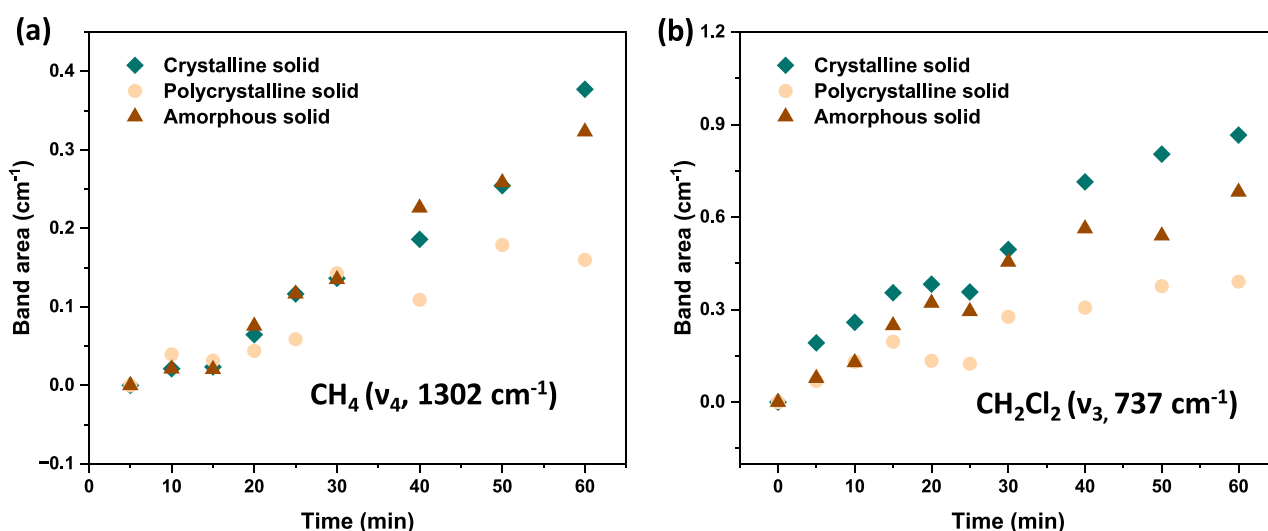


Figure 6. (a) Normalized integrated area of the ν_4 band of methane as a function of irradiation time. (b) Normalized integrated area of the ν_3 band of dichloromethane with irradiation time. Three phases of ice were irradiated for 60 min, and IR spectra were taken at 5 min intervals.

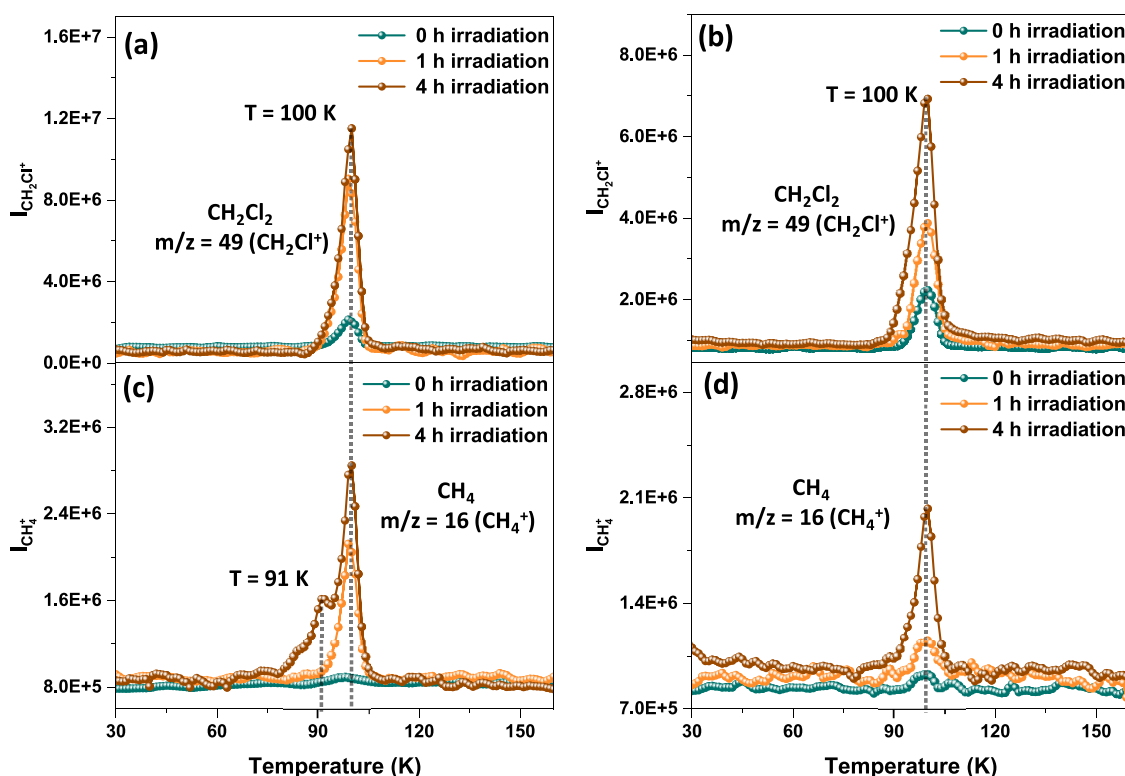


Figure 7. TPD-MS spectra of the photoproducts (CH_4 , CH_2Cl_2) formed by the irradiation of 63 ML of crystalline (a, c) and polycrystalline (b, d) methyl chloride for 0, 1, and 4 h. The sublimation profiles using integrated ion counts in (a, b) at $m/z = 49$ (CH_2Cl^+ due to CH_2Cl_2) and (c, d) at $m/z = 16$ (CH_4^+) are plotted.

enables the observation of sublimed products by TPD. Figure S9 shows the TPD mass spectrum for the major photoproducts hydrogen chloride ($m/z = 36$), dichloromethane ($m/z = 49$), and methane ($m/z = 16$). All the molecules desorb at 99 K, along with methyl chloride

Comparison of Photoproducts Formation and Trapping of Intermediates. We compared the efficiency of photoproduct formation in three distinct solids of methyl chloride, namely, amorphous, crystalline, and polycrystalline. Photoirradiation was performed on these solids at 10 K for a duration of 60 min, with RAIR spectra being recorded at 5 min

intervals. Figure 6 compares the formation of methane and dichloromethane, the major photoproducts resulting from the radical association (shown in Figure 3) within these three condensed phases. Abundances were calculated by integrating the band areas corresponding to methane (ν_4 , 1302 cm^{-1}) and dichloromethane (ν_3 , 737 cm^{-1}). The time-dependent areas due to methane and dichloromethane were calculated and subsequently normalized with respect to the C–Cl rocking (ν_6 , 1018 cm^{-1}) band of methyl chloride. For this normalization, the area under the curve (ν_6 , 1018 cm^{-1} band) for methyl chloride in the three solid phases was considered to be 1 cm^{-1}

before the radiation process. After normalization, the band areas of products of different types of ice versus time of irradiation are shown in Figure 6. Amorphous solids offer a conducive environment for enhanced product formation, primarily attributed to the augmented diffusion and tunneling of radicals within the porous matrix, a phenomenon not possible in crystalline solids.^{41–44} Here, a carefully created crystalline solid shows an equal or larger quantity of photoproducts than those in its amorphous and polycrystalline state. In the astrochemical model, the kinetics of reactions are influenced by reaction barriers and diffusion barriers. When there are no reaction barriers and the reactants are well-aligned, reactions are assumed to occur with high efficiency.⁷ This assumption is commonly applied to radical–radical reactions. The higher methane and dichloromethane production in crystalline than polycrystalline materials could be because radical migration is feasible in periodic crystalline materials. However, polycrystalline solids are composed of crystal domains with existing crystalline grain boundaries, and these grain-bound molecules play a vital role in the process of photolysis.⁴⁵ The presence of a thermal energy barrier on these boundaries is crucial, as it hinders radicals from moving between different crystalline grains. Consequently, the diffusion of intermediates is impeded, leading to the entrapment of all of the radicals within the boundaries themselves.

The phenomenon of extended irradiation leading to the conversion of crystalline solids into their amorphous analog has been widely established in the literature.^{46,47} A long-term irradiation experiment was carried out to investigate the consequences of the intermediates upon the amorphization of crystalline and polycrystalline solids. In this experiment, we irradiated the crystalline and polycrystalline ice for 4 h and compared it with the sample of 1 h irradiation using TPD-MS. Figure 7a,c shows the mass spectra of desorbed dichloromethane and methane before and after the irradiation of crystalline methyl chloride for 1 and 4 h. It is worth noting that the peak at 100 K for m/z 49 (Figure 7a,b) in the before irradiation spectrum represents the mass fragment from the methyl chloride reactant. In the spectrum collected after 1 h of irradiation, the desorption peaks of dichloromethane and methane at 100 K coincide with that of methyl chloride, and this is due to the small amount of photoproduct, which is trapped in the methyl chloride ice matrix. In Figure 7a, no specific changes have been detected other than an increase in dichloromethane. In the case of methane (Figure 7c), molecular volcano-like peaks were observed at 91 K in the 4 h irradiation experiment.^{48,49} Here, methane formation increased in the crystalline solid, which accumulated in specific locations. It is obvious that molecular mobility will be high prior to the desorption temperature in methyl chloride from its solid. Due to this high mobility, the accumulated methane molecules desorb earlier than methyl chloride as the methane desorption temperature is lower than that of methyl chloride.

Surprisingly, more intriguing results were observed when polycrystalline methyl chloride was irradiated for 4 h. The formation of dichloromethane (as shown in Figure 7b) increased by approximately 2 times, while methane (as shown in Figure 7d) increased by approximately 3 times when the irradiation time was extended from 1 to 4 h. This difference in product formation can be attributed to the transition of polycrystalline to the amorphous nature of methyl chloride during long-term irradiation, which removes the grain boundaries in the ice matrix. Consequently, the trapped

intermediates at the crystallite boundaries in the polycrystalline solid diffuse through the matrix and facilitate the formation of photoproducts. These results demonstrate strong agreement with our previous claim regarding the intermediate entrapment in polycrystalline solids.

This study presents a new direction in our understanding of molecular materials in space and their fate upon photoirradiation. Such photochemistry in molecular solids could make each of the distinct phases of any molecular solid an admixture of different species. In the course of time, an increase in the number of reaction products leads to the collapse of the crystallites, leading to an amorphous matrix. Therefore, photochemistry becomes an important factor in affecting the morphology of interstellar organics.

CONCLUSIONS

This study provides evidence for the formation of amorphous, crystalline, and polycrystalline methyl chloride via three different paths, using RAIRS in UHV ($\sim 5 \times 10^{-10}$ mbar) at low temperature (10–90 K), conditions analogous to ISM. The photochemistry of the methyl chloride solid was studied using a deuterium lamp (VUV source). The photoproducts were detected by RAIRS and SIMS in the solid state and by TPD-MS in the gas phase. The result of irradiation of three solid phases found that the formation of photoproducts is most facile for crystalline solid than for amorphous followed by polycrystalline. This is due to the feasibility of diffusion of the reactants and intermediates in crystalline solid compared to the amorphous and polycrystalline solids. Due to the existence of crystalline boundaries in polycrystalline solids, the intermediates are trapped at the interfaces of grains. However, long-term irradiation leads to the removal of discontinuity in the polycrystalline solid, which leads to the increased concentration of photoproducts accumulating in the ice matrix. This phenomenon becomes evident through the amplified desorption of photoproducts in TPD-MS. This study adds fresh spectroscopic data in the photochemistry of condensed methyl chloride molecules in ISM and provides a possible mechanistic interpretation that provides a scope for future investigations.

ASSOCIATED CONTENT

Supporting Information

The Supporting Information is available free of charge at <https://pubs.acs.org/doi/10.1021/acs.jpcc.3c05889>.

Temperature and time-dependent RAIRS, TPD-MS spectra, and SIMS spectrum of condensed methyl chloride (PDF)

AUTHOR INFORMATION

Corresponding Author

Thalappil Pradeep – Department of Science and Technology Unit of Nanoscience (DST UNS) and Thematic Unit of Excellence (TUE), Department of Chemistry, Indian Institute of Technology Madras, Chennai 600036, India; International Centre for Clean Water, IITM Research Park, Chennai 600113, India; orcid.org/0000-0003-3174-534X; Email: pradeep@iitm.ac.in

Authors

Bijesh K. Malla – Department of Science and Technology Unit of Nanoscience (DST UNS) and Thematic Unit of Excellence

(TUE), Department of Chemistry, Indian Institute of Technology Madras, Chennai 600036, India

Gaurav Vishwakarma – Department of Science and Technology Unit of Nanoscience (DST UNS) and Thematic Unit of Excellence (TUE), Department of Chemistry, Indian Institute of Technology Madras, Chennai 600036, India

Soham Chowdhury – Department of Science and Technology Unit of Nanoscience (DST UNS) and Thematic Unit of Excellence (TUE), Department of Chemistry, Indian Institute of Technology Madras, Chennai 600036, India

Complete contact information is available at:
<https://pubs.acs.org/10.1021/acs.jpcc.3c05889>

Author Contributions

B.K.M. and T.P. designed the experiments, B.K.M, G.V., and S.C. performed the experiments and analyzed the results. T.P. proposed the project and supervised the progress. The manuscript was written with the contributions of all authors.

Notes

The authors declare no competing financial interest.

ACKNOWLEDGMENTS

We acknowledge the Science and Engineering Research Board (SERB), Department of Science and Technology (DST), and Government of India for support. T.P. acknowledges funding from the Centre of Excellence on Molecular Materials and Functions under the Institution of Eminence scheme of IIT Madras. B.K.M. thanks the Council of Scientific and Industrial Research (CSIR) for his research fellowship. G.V. and S.C. thanks IITM for their research fellowships.

REFERENCES

- (1) Arumainayagam, C. R.; Garrod, R. T.; Boyer, M. C.; Hay, A. K.; Bao, S. T.; Campbell, J. S.; Wang, J.; Nowak, C. M.; Arumainayagam, M. R.; Hodge, P. J. Extraterrestrial Prebiotic Molecules: Photochemistry vs. Radiation Chemistry of Interstellar Ices. *Chem. Soc. Rev.* **2019**, *48* (8), 2293–2314.
- (2) Hama, T.; Watanabe, N. Surface Processes on Interstellar Amorphous Solid Water: Adsorption, Diffusion, Tunneling Reactions, and Nuclear-Spin Conversion. *Chem. Rev.* **2013**, *113* (12), 8783–8839.
- (3) Hollis, J. M.; Lovas, F. J.; Jewell, P. R.; Coudert, L. H. Interstellar Antifreeze: Ethylene Glycol. *Astrophys. J.* **2002**, *571* (1), L59–L62.
- (4) Cernicharo, J.; Heras, A. M.; Tielens, A. G. G. M.; Pardo, J. R.; Herpin, F.; Guélin, M.; Waters, L. B. F. M. Infrared Space Observatory's Discovery Of C₄H₂C₆H₂ And Benzene in Crl 618. *Astrophys. J.* **2001**, *546* (2), L123–L126.
- (5) Cami, J.; Bernard-Salas, J.; Peeters, E.; Malek, S. E. Detection of C₆₀ and C₇₀ in a Young Planetary Nebula. *Science* (80-) **2010**, *329* (5996), 1180–1182.
- (6) Cernicharo, J.; Agúndez, M.; Cabezas, C.; Tercero, B.; Marcelino, N.; Pardo, J. R.; De Vicente, P. Pure Hydrocarbon Cycles in TMC-1: Discovery of Ethynyl Cyclopropenyldiene, Cyclopentadiene, and Indene. *Astron. Astrophys.* **2021**, *649*, L15.
- (7) Öberg, K. I. Photochemistry and Astrochemistry: Photochemical Pathways to Interstellar Complex Organic Molecules. *Chem. Rev.* **2016**, *14*, 9631–9663.
- (8) Fayolle, E. C.; Öberg, K. I.; Jørgensen, J. K.; Altwegg, K.; Calcutt, H.; Müller, H. S. P.; Rubin, M.; van der Wiel, M. H. D.; Bjerkeli, P.; Bourke, T. L.; Coutens, A.; van Dishoeck, E. F.; Drozdovskaya, M. N.; Garrod, R. T.; Ligterink, N. F. W.; Persson, M. V.; Wampfler, S. F.; Balsiger, H.; Berthelier, J. J.; De Keyser, J.; Fiethe, B.; Fuselier, S. A.; Gasc, S.; Gombosi, T. I.; Sémon, T.; Tzou, C. Y.; et al. Protostellar and Cometary Detections of Organohalogens. *Nat. Astron.* **2017**, *1* (10), 703–708.
- (9) Keppler, F.; Harper, D. B.; Greule, M.; Ott, U.; Sattler, T.; Schöler, H. F.; Hamilton, J. T. G. Chloromethane Release from Carbonaceous Meteorite Affords New Insight into Mars Lander Findings. *Sci. Rep.* **2014**, *4* (1), 1–11.
- (10) Segura, A.; Kasting, J. F.; Meadows, V.; Cohen, M.; Scalo, J.; Crisp, D.; Butler, R. A. H.; Tinetti, G. Biosignatures from Earth-like Planets around M Dwarfs. *Astrobiology* **2005**, *5* (6), 706–725.
- (11) Nalezinski, R.; Bradshaw, A. M.; Knorr, K. A Vibrational Spectroscopy Study of the Orientational Ordering in CH₃Cl Monolayers Physisorbed on Graphite. *Surf. Sci.* **1997**, *393* (1–3), 222–230.
- (12) Burbank, R. D. The Crystal Structure of Methyl Chloride At-12501. *J. Am. Chem. Soc.* **1953**, *75*, 1211–1214, DOI: [10.1021/ja01101a059](https://doi.org/10.1021/ja01101a059).
- (13) Stoppa, P.; Pietropolli Charmet, A.; De Lorenzi, A.; Tamassia, F.; Melosso, M.; Cané, E.; Dore, L.; Puzzarini, C. High Resolution FTIR Study of the ν_5 , ν_6 , and ν_9 Fundamental Bands of CH₂D³⁷Cl. *J. Quant. Spectrosc. Radiat. Transfer* **2021**, *270*, No. 107719.
- (14) Bag, S.; Bhui, R. G.; Methikkalam, R. R. J.; Pradeep, T.; Kephart, L.; Walker, J.; Kuchta, K.; Martin, D.; Wei, J. Development of Ultralow Energy (1–10 eV) Ion Scattering Spectrometry Coupled with Reflection Absorption Infrared Spectroscopy and Temperature Programmed Desorption for the Investigation of Molecular Solids. *Rev. Sci. Instruments* **2014**, *85* (1), 1–7.
- (15) Vishwakarma, G.; Ghosh, J.; Pradeep, T. Desorption-Induced Evolution of Cubic and Hexagonal Ices in an Ultrahigh Vacuum and Cryogenic Temperatures. *Phys. Chem. Chem. Phys.* **2021**, *23* (41), 24052–24060.
- (16) Bartmess, J. E.; Georgiadis, R. M. Empirical Methods for Determination of Ionization Gauge Relative Sensitivities for Different Gases. *Vacuum* **1983**, *33* (3), 149–153.
- (17) Vishwakarma, G.; Malla, B. K.; Chowdhury, S.; Khandare, S. P.; Pradeep, T. Existence of Acetaldehyde Clathrate Hydrate and Its Dissociation Leading to Cubic Ice under Ultrahigh Vacuum and Cryogenic Conditions. *J. Phys. Chem. Lett.* **2023**, *14*, 5328–5334.
- (18) Lee, D. H.; Kang, H. Acid-Promoted Crystallization of Amorphous Solid Water. *J. Phys. Chem. C* **2018**, *122* (42), 24164–24170.
- (19) Dows, D. A. Vibrational Spectra of the Crystalline Methyl Halides. *J. Chem. Phys.* **1958**, *29* (3), 484–489.
- (20) Gobinda Bhui, R.; Rajan, R.; Methikkalam, J.; Bag, S.; Pradeep, T. Diffusion and Crystallization of Dichloromethane within the Pores of Amorphous Solid Water. *J. Phys. Chem. C* **2016**, *120* (25), 13474–13484, DOI: [10.1021/acs.jpcc.6b00436](https://doi.org/10.1021/acs.jpcc.6b00436).
- (21) Nesheva, D.; Bineva, I.; Levi, Z.; Aneva, Z.; Merdzhanova, T.; Pivin, J. C. Composition, Structure and Annealing-Induced Phase Separation in SiOx Films Produced by Thermal Evaporation of SiO in Vacuum. *Vacuum* **2002**, *68* (1), 1–9.
- (22) Philip, J.; Gnanaprakash, G.; Panneerselvam, G.; Antony, M. P.; Jayakumar, T.; Raj, B. Effect of Thermal Annealing under Vacuum on the Crystal Structure, Size, and Magnetic Properties of ZnFe₂O₄ Nanoparticles. *J. Appl. Phys.* **2007**, *102* (5), 54305.
- (23) Lilach, Y.; Asscher, M. Compression and Caging of CD₃Cl by H₂O Layers on Ru(0001). *J. Chem. Phys.* **2002**, *117* (14), 6730–6736.
- (24) Makino, T.; Zulaehah, S.; Gueriba, J. S.; Diño, W. A.; Okada, M. CH₃Cl/Cu(410): Interaction and Adsorption Geometry. *J. Phys. Chem. C* **2018**, *122* (22), 11825–11831.
- (25) Takeuchi, H.; Harada, I.; Shimanouchi, T. Anomalous Splitting Pattern of the ν_3 Vibrational Band of Crystalline Methyl Chloride: Chlorine Isotopic Effects. *Chem. Phys. Lett.* **1976**, *43* (3), 516–519.
- (26) Duncan, J. L.; McKean, D. C.; Mallinson, P. D.; McCulloch, R. D. Infrared Spectra of CHD₂Cl and CHD₂CCH and the Geometries of Methyl Chloride and Propyne. *J. Mol. Spectrosc.* **1973**, *46* (2), 232–239.
- (27) Lin, M.-Y.; Huang, T.-P.; Wu, P.-Z.; Chin, C.-H.; Wu, Y.-J. Formation of Halogen-Bearing Species. II. Irradiation of Chloromethane in Carbon Monoxide Ice with VUV Light and Electrons. *Astrophys. J.* **2020**, *888* (1), 39.

- (28) Morrison, A. M.; Flynn, S. D.; Liang, T.; Doublerly, G. E. Infrared Spectroscopy of $(\text{HCl})_m(\text{H}_2\text{O})_n$ Clusters in Helium Nanodroplets: Definitive Assignments in the HCl Stretch Region. *J. Phys. Chem. A* **2010**, *114* (31), 8090–8098.
- (29) Öberg, K. I.; Garrod, R. T.; Van Dishoeck, E. F.; Linnartz, H. Formation Rates of Complex Organics in UV Irradiated CH_3OH -Rich Ices - I. Experiments. *Astron. Astrophys.* **2009**, *504* (3), 891–913.
- (30) Lin, J. J.; Chen, Y.; Lee, Y. Y.; Lee, Y. T.; Yang, X. Photodissociation Dynamics of CH_3Cl at 157.6 nm: Evidence For. *Chem. Phys. Lett.* **2002**, *361* (5–6), 374–382.
- (31) Matsumi, Y.; Tonokura, K.; Kawasaki, M.; Inoue, G.; Satyapal, S.; Bersohn, R. Erratum: Fine Structure Branching Ratios and Doppler Spectroscopy of Chlorine Atoms from the Photodissociation of Alkyl Chlorides and Chlorofluoromethanes at 157 and 193 nm [J. Chem. Phys. *94*, 2669 (1991)]. *J. Chem. Phys.* **1992**, *97* (7), 5261.
- (32) Kawasaki, M.; Kasatani, K.; Sato, H.; Shinohara, H.; Nishi, N. Photodissociation of Molecular Beams of Halogenated Hydrocarbons at 193 nm. *Chem. Phys.* **1984**, *88* (1), 135–142.
- (33) Brownsword, R. A.; Hillenkamp, M.; Laurent, T.; Vatsa, R. K.; Volpp, H. R.; Wolfrum, J. Photodissociation Dynamics of the Chloromethanes at the Lyman- α Wavelength (121.6 nm). *J. Chem. Phys.* **1997**, *106* (4), 1359.
- (34) Amaral, G.; Xu, K.; Zhang, J. H-Atom Product Channels in the Photodissociation of CH_3Cl , CH_3Br , and CH_3I at 121.6 nm. *J. Phys. Chem. A* **2001**, *105* (7), 1115–1120, DOI: 10.1021/jp0028507.
- (35) Lilach, Y.; Asscher, M. Photochemistry of Caged Molecules: $\text{CD}_3\text{Cl@Ice}$. *J. Chem. Phys.* **2003**, *119* (1), 407–412.
- (36) Ayoub, Y.; Asscher, M. Photochemistry of Ethyl Chloride Caged in Amorphous Solid Water. *Phys. Chem. Chem. Phys.* **2008**, *10* (32), 6486–6491.
- (37) Gilton, T. L.; Dehnostel, C. P.; Cowin, J. P. Electron Transmission through Layers of H_2O and Xe in the Ultrahigh Vacuum Photoreduction of CH_3Cl on Ni(111). *J. Chem. Phys.* **1989**, *91* (3), 1937–1938.
- (38) Kang, H. Chemistry of Ice Surfaces. Elementary Reaction Steps on Ice Studied by Reactive Ion Scattering. *Acc. Chem. Res.* **2005**, *38* (12), 893–900.
- (39) Park, S. C.; Maeng, K. W.; Pradeep, T.; Kang, H. Reactive Ion Scattering from Pure and Mixed HCl, NH_3 , and D_2O Surfaces. *Nucl. Instruments Methods Phys. Res. Sect. B Beam Interact. with Mater. Atoms* **2001**, *182* (1–4), 193–199.
- (40) Kim, Y.; Moon, E.; Shin, S.; Kang, H. Acidic Water Monolayer on Ruthenium(0001). *Angew. Chem.* **2012**, *124* (51), 12978–12981.
- (41) Andersson, S.; Al-Halabi, A.; Kroes, G. J.; van Dishoeck, E. F. Molecular-Dynamics Study of Photodissociation of Water in Crystalline and Amorphous Ices. *J. Chem. Phys.* **2006**, *124* (6), 64715.
- (42) Yabushita, A.; Inoue, Y.; Senga, T.; Kawasaki, M.; Sato, S. Photodissociation of Chlorine Molecules Adsorbed on Amorphous and Crystalline Water Ice Films. *J. Phys. Chem. B* **2002**, *106* (12), 3151–3159.
- (43) Yabushita, A.; Hama, T.; Iida, D.; Kawasaki, M. Hydrogen Peroxide Formation Following the Vacuum Ultraviolet Photodissociation of Water Ice Films at 90 K. *J. Chem. Phys.* **2008**, *129* (1), 14709.
- (44) Noble, J. A.; Michoulier, E.; Aupetit, C.; Mascetti, J. Influence of Ice Structure on the Soft UV Photochemistry of PAHs Embedded in Solid Water. *Astron. Astrophys.* **2020**, *644*, A22.
- (45) Watanabe, N. Behaviour of Radicals on Interstellar Dust Analogues. *Proc. Int. Astron. Union* **2019**, *15* (S350), 116–122.
- (46) Kouchi, A.; Kuroda, T. Amorphization of Cubic Ice by Ultraviolet Irradiation. *Nat.* **1990**, *344* (6262), 134–135.
- (47) Tachibana, S.; Kouchi, A.; Hama, T.; Oba, Y.; Piani, L.; Sugawara, I.; Endo, Y.; Hidaka, H.; Kimura, Y.; Murata, K.-I.; et al. Liquid-like Behavior of UV-Irradiated Interstellar Ice Analog at Low Temperatures. *Sci. Adv.* **2017**, *3* (9), No. ea02538, DOI: 10.1126/sciadv.aao2538.
- (48) Malla, B. K.; Vishwakarma, G.; Chowdhury, S.; Selvarajan, P.; Pradeep, T. Formation of Ethane Clathrate Hydrate in Ultrahigh Vacuum by Thermal Annealing. *J. Phys. Chem. C* **2022**, *2022*, 17983–17989.
- (49) Ramakrishnan, S.; Sagi, R.; Mahapatra, N.; Asscher, M. Effect of Coadsorbed Oxygen on the Photochemistry of Methane Embedded in Amorphous Solid Water. *J. Phys. Chem. C* **2018**, *122* (27), 15287–15296.